Structural and magnetic anisotropies of Fe/ZnSe(001) thin films

M. Marangolo, F. Gustavsson,* G. M. Guichar, M. Eddrief, J. Varalda,† and V. H. Etgens
Laboratoire de Minéralogie et de Cristallographie de Paris-CNRS, Universités Paris VI et VII, IPGP, 4, Place Jussieu, F-75252 Paris, Cédex 05, France

M. Rivoire and F. Gendron
Laboratoire des Milieux Désordonnés et Hétérogènes (LDMH), CNRS, Université Paris VI, 4, Place Jussieu, F-75252 Paris, Cedex 05, France

H. Magnan
Laboratoire pour l'Utilisation du Rayonnement Electromagnétique, CNRS, Université de Paris-Sud Bat. 209-D, 91405 Orsay, France and Service de Physique et Chimie des Surfaces et Interfaces, DSM/DRECAM, CEA/Saclay, 91191 Gif-sur-Yvette, France

D. H. Mosca
Departamento de Física– UFPR, C. P. 19091, 81531-990 Curitiba PR, Brazil

J.-M. George
Unité Mixte de Physique CNRS – Thales Domaine Corbeville, 91404 Orsay, France
(Received 17 February 2004; revised manuscript received 21 June 2004; published 11 October 2004)

The morphology, the atomic structure, and the strain of very thin Fe epilayers grown on ZnSe(001) have been studied by combined scanning tunnel microscope (STM) and extended x-ray-absorption fine-structure experiments. It turns out that the crystal structure of the flat and anisotropic islands (up to 5 monolayers) and terraces (higher coverages) observed by STM is close to bulk iron but affected by a weak out-of-plane tetragonal distortion. Strain measurements and magnetic anisotropy constants of very thin films obtained by ferromagnetic resonance measurements allow us to conclude that the important out-of-plane anisotropy term is determined by the interface atomic structure. Finally, we put forward two hypotheses to explain why the measured out-of-plane anisotropy is one order of magnitude larger than the [110] in-plane anisotropy. The *former* is related to a disordered configuration of iron and zinc atoms between bonding and antibonding sites at the interface. The *latter* hypothesis is related to the direction of the demagnetization field due to the morphology of iron films.

DOI: 10.1103/PhysRevB.70.134404 PACS number(s): 75.70.−i, 75.30.Gw, 68.55.−a, 76.50.+g

I. INTRODUCTION

One of the material science challenges today consists in combining magnetic and semiconductor epilayers to obtain an efficient electrical injection of spin-polarized carriers.[1] A well-characterized and spin-injection efficient hybrid magnetic metal/semiconductor heterostructures could lead to devices using not only the charge of electrons but also their spin. The development of these devices needs the understanding, the reproducibility, and the tailoring of film growth and a careful characterization of its magnetic properties.

A promising system is Fe epitaxied on the wide band-gap semiconductor ZnSe(001).[2–4] The Fe/ZnSe(001) heterostructure has a low lattice mismatch (1.1%) taking two Fe lattices matching one of ZnSe and, more importantly, the reactivity is lower in respect to other semiconductors such as GaAs, Si, or Ge.[5] In addition, it is feasible to achieve coherent spin transfer with high efficiency across the GaAs/ZnSe interface[6] and Jiang *et al.* found tunneling magnetoresistance values of 10% at room temperature.[7]

Recently, we have shown that the interface is magnetically sharp with Fe magnetic moments being similar or even larger than bulk[8] and we have also evaluated the Fe/ZnSe(001) Schottky-barrier height by photoelectron emission spectroscopy.[9] These works have permitted us to state that the Fe/ZnSe interface is essentially abrupt with minimal chemical contact interaction between the top-most atomic layers of the ZnSe epilayer and Fe atoms.

In a pioneering work Jonker and Prinz[10] showed by Auger electron diffraction that the film growth followed a predominantly layer by layer mode with no significant clustering or multilayer island formation. Here we present scanning tunnel microscope (STM) images of iron epilayers on ZnSe(001) at low Fe coverages (1–7 monolayers). Next, we have used the sensitivity of extended x-ray-absorption fine-structure (EXAFS) experiments to determine the atomic structure and to measure strain of the iron thin film. Then, we correlate structural findings with the magnetic anisotropy constants measured by the angular dependence of the resonance field in ferromagnetic resonance (FMR). Our aim was to understand the microscopic origin of UMA (uniaxial magnetic anisotropy) observed for thin Fe layers. Indeed, similarly to Fe/GaAs(001), Fe/ZnSe(001) presents an unexpected in-plane UMA with an [110] easy axis. A number of mechanisms can lead to UMA in magnetic thin film, including shape anisotropy, epitaxial strain, step anisotropies, or interfacial compound formation. In particular, UMA in Fe/GaAs(001) has been exensively studied by many

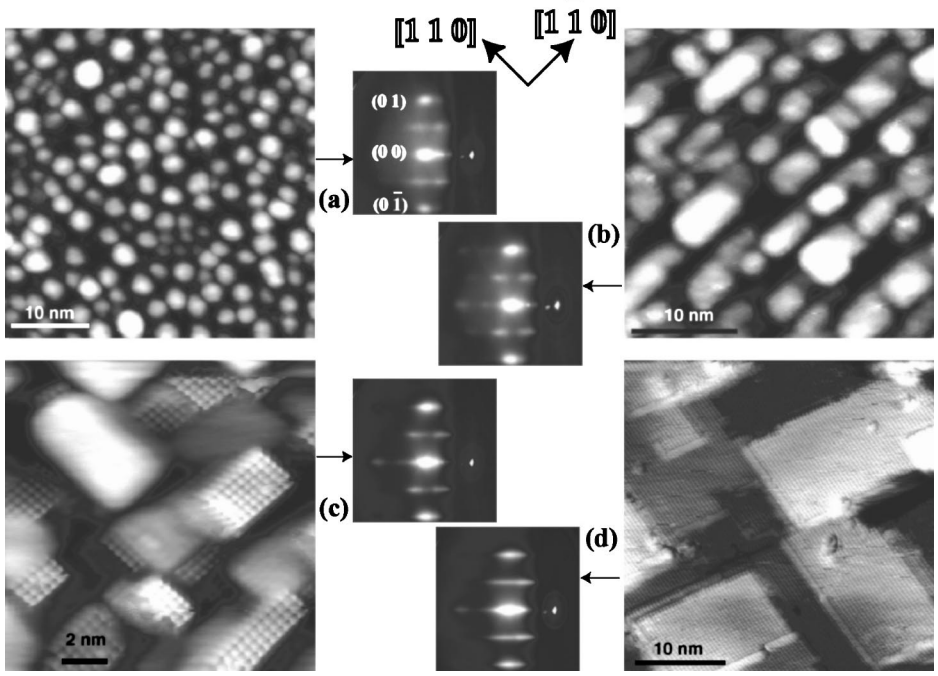

FIG. 1. STM images at different Fe coverages (1, 3, 5, and 7 ML's) on a $c(2\times2)$ reconstructed Zn-terminated ZnSe(001) surface. RHEED diagrams are also presented. (a) At 1 ML we observe flat discs, with an average diameter of ~30 Å and a maximum thickness of 2 ML's. (b) At 3 ML's, islands present more straight edges along the ⟨110⟩ directions of the substrate. (c) At 5 ML's, the corrugation is released by a two-dimensional coalescence: large, atomically flat rectangular terraces cover the surface. The atomic resolution can be achieved on this surface, where the reconstruction corresponds to a Fe(2×2) Se-induced reconstruction. At 7 ML's the island coalescence is accomplished and the film presents long-range order. The terrace step height is about 1.6 Å. The (2×2) reconstruction of the segregating Se is still well identified.

groups:[11] it turns out that UMA is independent of the GaAs surface reconstructions indicating that strain has little effect.[12] Recently, O. Thomas *et al.*,[13] by grazing x-ray-diffraction measurements, concluded that UMA in Fe/GaAs is caused by an interface anisotropy. Moreover, E. Sjöstedt *et al.*[14] calculated that the UMA in Fe/ZnSe(001) is produced by the directional covalent bonds at the interface, even without atomic relaxations.

In this paper, we will compare the magnetoelastic term due to strain measured by EXAFS and the contribution from the interface term. It will be shown that this latter term, due to sp^3-like tetrahedral bonds from the substrate to the Fe atoms at the interface, is the more important and breaks the fourfold symmetry of iron.

This work is organized in two main sections: the first concerns the structural studies (STM and EXAFS) and the second the magnetic properties (FMR).

II. SECTION I: STM OBSERVATION OF THE Fe/ZnSe(001) SURFACE

A. Experimental

The samples were prepared by molecular-beam epitaxy (MBE) in a multichamber system. First, a GaAs buffer layer was deposited on GaAs(001) substrates using standard growth conditions,[15] followed by transfer to a II-VI chamber for ZnSe growth using a two-step procedure.[16] At the end, a $c(2\times2)$ Zn-rich surface[17] was stabilized on top of a 100-Å pseudomorphic ZnSe epilayer. The Fe was grown *in situ* at 180 °C with a rate of about 1 monolayer (ML) per minute at a base pressure below 3×10^{-10} mbar. During the Fe growth, the reflection high-energy electron diffraction (RHEED) diagram changes from the usual streaky [two-dimensional (2D] ZnSe diagram to a diffuse one around 0.5 ML, followed by elongated spots characteristic of Fe above 1 ML (see Fig. 1). Indeed, one monolayer of Se is always found floating at the growth front independently of the Fe film thickness, leading to a 2×2 reconstruction observed on RHEED diagrams.[2,18] *In situ* scanning tunneling microscopy (STM) images were collected at room temperature in constant current mode.

B. Results

STM images at different Fe coverages (1, 3, 5, and 7 ML's) on ZnSe(001) $c(2\times2)$ are shown in Fig. 1. At 1 ML, isotropic Fe islands cover the ZnSe(001) surface. Observed discs are flat, with an average diameter of ~30 Å and a height of about 2 ML. The pronounced nonlinearity of scanning tunneling spectroscopy (STS) measurements indicate that topographic minima correspond to the semiconductor surface, as opposed to the metallic character of the islands. This confirms the XPS results presented in Ref. 9.

At 3 ML's, islands present more straight edges along the (110) directions of the substrate. They are anisotropic and elongated along the $[1\bar{1}0]$ direction. A similar behavior has been observed for Fe grown on GaAs(001) (2×4),[19] where

the preferred coalescence direction coincides with the $[1\bar{1}0]$ oriented As-dimer rows. The origin of this anisotropy was suggested to be correlated with kinetic anisotropies, i.e., a faster diffusion along the As dimer rows. In the present case, however, the surface reconstruction is normally symmetric [Zn rich $c(2\times2)$] (Ref. 17) and therefore an isotropic coalescence should intuitively be expected. Another plausible anisotropic contribution comes from the unsatisfied unidirectional sp^3 bonds on the ZnSe surface. The $c(2\times2)$ reconstruction represents only a half Zn monolayer surface leaving Se atoms exposed in the subsurface layer.[17] Since Fe would prefer to bond to Se rather than to Zn, the $[1\bar{1}0]$ oriented Se *sp*3 bonds would favor Fe to coalesce along this direction.[20]

With increasing Fe thickness (5 ML's), the corrugation switches to a two-dimensional coalescence: large, atomically flat rectangular terraces cover the surface. The atomic resolution can be obtained on this surface, with the observed 2×2 reconstruction being induced by the Se floating monolayer at the Fe growth front.

At 7 ML's, the island coalescence is accomplished and the film presents long-range order: (i) a metallic signal is recorded onto the entire sample surface at 7 ML's thus confirming island coalescence. (ii) The iron surface is flat with atomically resolved terraces with sizes reaching 300 Å. The terrace step height is of about 1.6 Å that corresponds quite well to the value expected for Fe (1.43 Å). (iii) The (2×2) reconstruction of the segregating Se is still well identified.

In the following, we discuss the inner structure of the islands observed on the surface in the case of very thin Fe films. In order to characterize this system as a function of Fe covering we performed extended x-ray absorption fine-structure (EXAFS) experiments.

C. EXAFS experiments

EXAFS consists of measuring the absorption coefficient of the sample as a function of the incoming photon energy. Oscillations of the absorption coefficient after the Fe *K*-absorption edge reflect the structure and the local order around this excited atom. EXAFS is a very well suited technique for the study of ultrathin epitaxial films because of its atom selectivity and the linear polarization of the x rays of synchrotron radiation. Indeed, EXAFS oscillations depend on the polarization direction of the x rays with respect to the crystallographic axis. Then, normal (NI) and grazing (GI) incidence experiments (linear polarization of the x ray parallel to the film plane or at about 75° from the film plane) allow us to measure both in-plane and out-of-plane lattice parameters and to detect an eventual epitaxy induced distortion of the epilayer.

D. Experimental procedure

Experiments were carried out at the Laboratoire pour l'Utilisation du Rayonnement Electromagnétique (LURE, France), on the wiggler beam line of the DCI storage ring at the Fe *K*-edge (7110 eV). The spectra were recorded in the fluorescence yield mode, with the sample cooled at 77 K. For these experiments, the ZnSe/GaAs(001) samples have been capped with an amorphous Se layer, a technique very efficient for preventing contamination during air transport.[8,9,17] Once introduced in the EXAFS UHV setup, they were slowly heated up to 350 °C in order to remove the Se capping layer and to stabilize the $c(2\times2)$ Zn terminated surface. Next, Fe was deposited at 180 °C from an *e*-beam evaporator with the thickness being controlled both by quartz microbalance and by the absorption edge (with a discrepancy lower than 50%). We prepared a new ZnSe sample for each Fe coverage and we recorded three EXAFS spectra, two in NI with the linear polarization either parallel to [110] or to $[1\bar{1}0]$ ZnSe axis, and one in GI with the linear polarization parallel to [001].

Probed samples thickness were 2, 4, and 27 ML's, and bulk iron (reference). A very low coverage thin film (0.8 ML) was also measured but only at normal incidence.

In this paper we fitted the inverse fourier transform (IFT) of the first peak of the Fourier Transform (FT) of the EXAFS oscillations[21] $[\chi(k)]$, using the classical EXAFS formula. This well-known procedure isolates the contribution of the first-nearest-neighbor shell and leads to an evaluation of the crystallographic parameters of the thin film. Then, the higher distant shells are simulated in the multiple-scattering approach by FEFF 6.0.[22]

E. Polarization dependence of the nearest-neighbors shell EXAFS signal

The absorption spectra recorded on five samples at normal (polarization parallel to [110]) and grazing incidences are shown in Fig. 2.

It is worth noting that, except at very low coverage (0.8 ML), the main EXAFS $\alpha-$Fe structures are observed in all the spectra. As a consequence, we can state that at 2 ML's iron grows in a bcc-like structure, even if at 2 and 4 ML's EXAFS structures at normal incidence seem slightly shifted towards high *k* values.

The Fourier transform of the EXAFS oscillations between $k=2.5$ and 12 Å gives a series of broad peaks corresponding to different shells of neighbors (see Fig. 3). The crystallographic parameters are obtained by fitting the IFT of the first peak for the normal and grazing incidence. The best fit is obtained with a body-centered-tetragonal (bct) structure. The parameters of this structure are

a: the distance between the scattering atom and the four atoms located in the same (001) plane;

c: the distance with the two neighbors on an axis perpendicular to the film plane;

d: the distance with the four first-nearest neighbors.

The first peak of the FT (between 1.5 and 2.8 Å) includes the three distances (*a*, *c*, and *d*) in a bct structure. The contribution of these bonds in the EXAFS signal depend on the direction of the polarization of the x rays, since each bond is weighted by a $\cos^2\alpha$ factor, where α is the angle between the bond and the polarization of the x rays. Indeed, whatever the x ray's angle of incidence, there are always two types of distances in the first peak of the FT: *a* and *d* in NI, and *c* and *d* in GI.[23] The number of first- and second-nearest neighbors is fixed at 8 and 6, respectively. In the fitting procedure, the

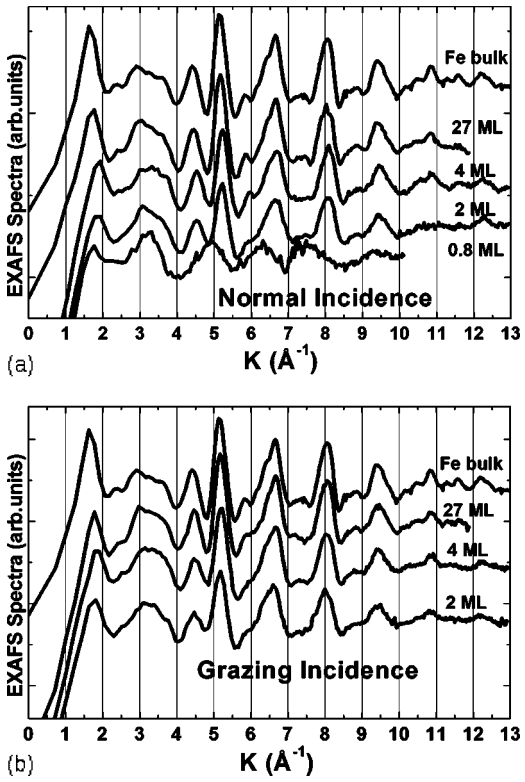

FIG. 2. Absorption spectra recorded on the five samples at the normal (a) and grazing incidences (b). We notice that, except at very low coverage (0.8 ML), the main EXAFS α-Fe structures are observed in all the collected spectra.

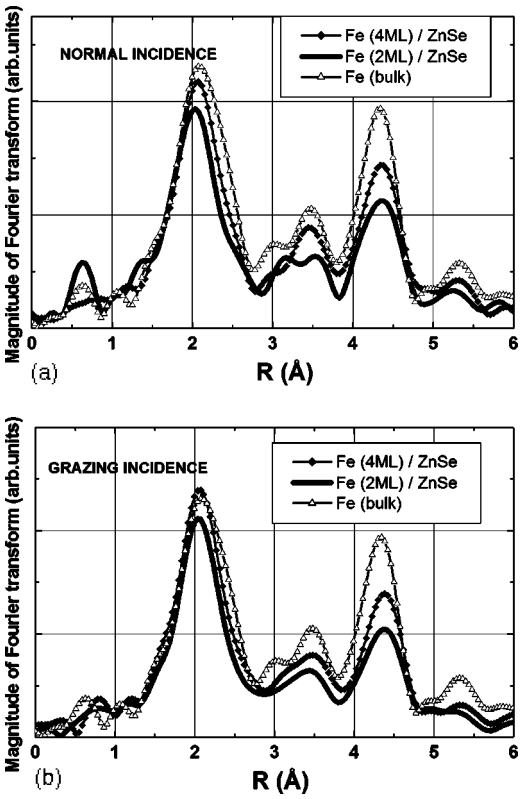

FIG. 3. Fourier transform of the measured EXAFS oscillations at different coverages at (a) normal incidence and (b) grazing incidence.

two spectra recorded in NI (respectively, polarization parallel to [110] and $[1\bar{1}0]$) give identical results in the experimental accuracy. We conclude then that the structure is not distorted in the (001) plane. More precisely, we report in Table I the differences between the measured parameters and the bulk Fe values (where $a=b=c=2.87$ Å), and the σ^2 factor that takes into account the thermal agitation and the static disorder. These results show unambiguously that, at low coverage, the Fe bcc structure is stretched by the epitaxy on the ZnSe (001) substrate, leading to a body-centered-tetragonal structure (bct) with $\Delta a<0$ (with $\Delta a=\Delta b$) and $\Delta c>0$.

The normal incidence measurements of 2- and 4-ML-thick films give a lattice contraction of a equal to -0.020 and −0.025 Å in comparison with bulk iron, respectively. This is consistent with epitaxy parameters: twice the lattice parameter of Fe ($2a_{\mathrm{Fe}}=5.732$ Å) exceeds the lattice parameter of ZnSe ($a_{\mathrm{ZnSe}}=5.669$ Å) by approximately 1.1%. Besides, from grazing incidence measurements it turns out that c is slightly elongated (+0.02 Å). The σ factor is larger for thin films indicating static disorder. Bulk values are recovered for the 27-ML-thick sample.

The tetragonal distortion due to epitaxy can be confirmed by the phase derivatives (PD) analysis of the experimental signal. Indeed, this differential method is very well suited for the detection of lattice deformations. G. Martens *et al.*[24] show that the difference between the mean distances of the two closer shells can be determined from the minimum of the phase derivative of EXAFS spectra. In Fig. 4 we report PD extracted from experimental data (4 ML's). We notice that minima of the phase derivatives of NI and GI signals are located at distinct positions, confirming the tetragonal distortion of the thin film. Using the same method (not shown here), we observed that at 27 ML's, this distortion is released.

F. Simulations of the EXAFS spectra

In order to compare with the EXAFS spectra, we have performed complete simulations of the polarization dependent x-ray-absorption spectra, starting from a Fe cluster built with the lattice parameters deduced from the nearest-neighbors analysis. This was done using the FEFF code, which calculates the absorption cross section in a multiple scattering.[22] At first sight, a simple FEFF simulation using the spherical bct Fe-cluster with the lattice parameters reported in Table I matches nicely with the Fourier transform of experimental results (see Fig. 5). Nevertheless, we tried to simulate the experimental spectra with a model of a real thin film, motivated by two observations: (i) STM images show that clusters are flat, elongated, extended, and a few monolayers thick (see Fig. 1). (ii) The broad peak at around 4.4 Å in Fig. 5 is lower in the experimental spectrum than in the simulation with the spherical cluster, indicating that the number of neighbors is reduced in comparison with bulk. As a consequence, EXAFS measurements must be sensitive to the Fe/ZnSe interface.

TABLE I. Differences between the measured parameters and the bulk Fe values (where $a=b=c=2.87$ Å), and the σ^2 factor that takes into account the thermal agitation and the static disorder. These results show unambiguously that, at low coverage, the Fe bcc structure is stretched by the epitaxy on the ZnSe(001) substrate, leading to a body-centered tetragonal structure (bct) with $\Delta a<0$ (with $\Delta a=\Delta b$) and $\Delta c>0$.

Coverage (ML)	First neighbors (Å) ±0.01 Å	σ^2(Å^2) Debye Waller	Second neighbors (Å) ±0.01 Å	σ^2(Å^2) Debye Waller a and c;
2	$\Delta d=0.000$	2×10^{-3}	$\Delta a=-0.020$;	6×10^{-3}
			$\Delta c=0.001$	8×10^{-3}
4	$\Delta d=-0.005$	1×10^{-3}	$\Delta a=-0.025$;	3×10^{-3}
			$\Delta c=0.02$	4×10^{-3}
27	$\Delta d=0.000$	1×10^{-3}	$\Delta a=0.000$;	2×10^{-3}
			$\Delta c=0.000$	2×10^{-3}
Bulk	reference	2.5×10^{-3}	reference	2.5×10^{-3}

As a consequence, we calculated the EXAFS spectra using a new cluster of an "ideal" thin film: the bulk semiconductor, terminated by a complete Se layer, is continued by five layers of Fe, where half of the atoms in the (001) planes are positioned at crystal sites of the zinc-blende structure, and half of the atoms are located in the corresponding voids (bonding and antibonding sites in the zinc-blende structure). The lattice parameters of iron thin films are the same as of bct bulk simulation discussed above. This structure (except the floating Se layer) is the same as the supercell used by Sjöstedt *et al.*[14] for *ab initio* calculations of the uniaxial magnetocrystalline anisotropy. Moreover, since experimentally we know that a Se layer floats on the surface leading to a 2×2 superstructure (see Fig. 1), we added Se atoms above half of the squares of the topmost Fe (001) layer. The distances between iron and selenium atoms at the interfaces ZnSe/Fe thin-film interface and iron thin-film/floating selenium layer interface) are fixed at 2.48 Å, i.e., the Fe-Se equilibrium distance.[20,25]

EXAFS spectra of all nonequivalent Fe atoms of the thin film were calculated by FEFF. The results for the normal and grazing incidences are shown in Fig. 5 (open squares). We notice that the FT spectra are slightly modified in comparison with the simulation with the spherical cluster. The peak at around 4.4 Å falls down to the GI experimental height due to the reduced thickness of the film. On the other hand, the NI calculated spectrum is characterized by a *broader peak at* 2 Å, surely due to the two Fe/Se interfaces of the thin film. Many attempts were made without better reproducing the experimental 2-Å peak feature: (i) the Fe/Se-terminated

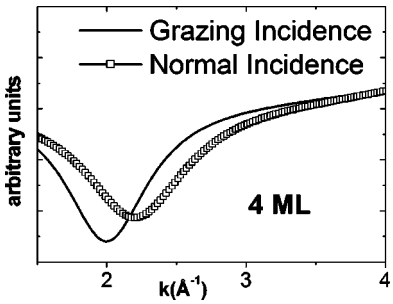

FIG. 4. Analysis of the phase derivatives of the experimental signal (4 ML's). We notice that minima of the phase derivatives of NI and GI signals are located at distinct positions, indicating a tetragonal distortion of the thin film.

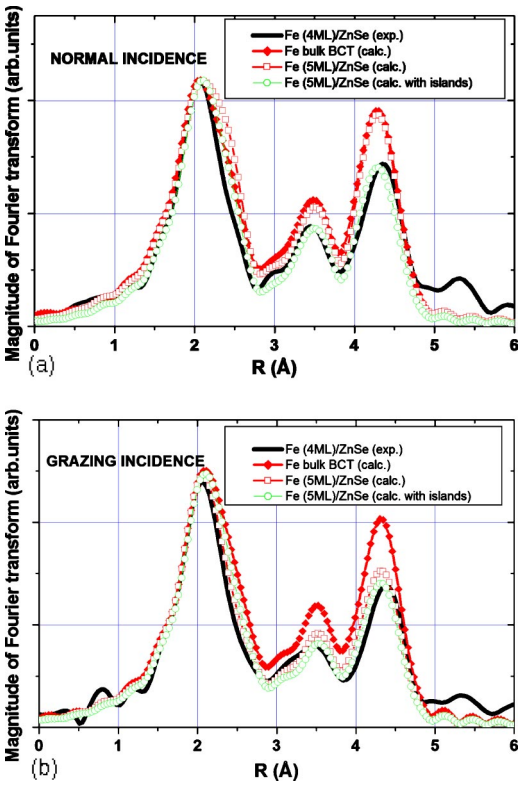

FIG. 5. (Color online) Comparison between measured and simulated spectra at the (a) normal and (b) grazing incidences. For simulated spectra obtained by FEFF 6.0: $T_{debye}=470°C$. Bulk iron contribution is calculated by a cluster of iron atoms in a bct structure (see parameters in Table I, 4 ML's). In the case of thin-film simulations: iron is epitaxied on ZnSe (001) ($a_{ZnSe}/2=2.825$ Å); the lattice parameters are the same of Table I (4 ML's) ; distance nearest-neighbor Fe-Se atoms at the interfaces =2.48 Å. We notice that the FT spectra are slightly modified with respect to bulk. Simulations called "with islands" are obtained taking into account the size and the morphology of iron clusters as observed by STM.

semiconductor interface was substituted with a Fe/Zn interface; (ii) the distances between atoms at interfaces were strongly modified; (iii) FT spectra were calculated using relaxed-atomic positions obtained by first-principles electronic calculations.[20]

In the following, we show that the 2-Å peak width is mainly due to the morphology of the thin film. First of all, we observe that in the GI simulation the 2-Å peak is not broadened as respect to bulk calculations and GI experiments, even if in this experimental geometry, spectra are more sensitive to the interface. We put forward the hypothesis that the "broading effect" due to the interface is canceled by another effect due to the small thickness of the iron film (5 ML's). A similar effect due to the reduced lateral size of Fe islands on the surface could narrow the experimental NI spectra. Indeed, as observed in STM images, at 2–5 ML's, the surface is characterized by flat, elongated, extended, and a few monolayers thick islands. Therefore the narrow 2-Å peak in the NI spectrum may be due to the presence of islands on the surface. In order to test this hypothesis, we have calculated EXAFS spectra of elongated Fe islands deposited on ZnSe. More precisely, for the calculation we use the same thin film described above and we cut it along the [110] direction. We then calculated the EXAFS spectra of all the Fe atoms sitting along the step, on its edges and very close to it, considering the cases of the polarization axis parallel and perpendicular to the artificial step edge. After that, we added the EXAFS contribution of "innerlike" and "steplike" Fe atoms, weighing with realistic coefficient extrapolated from the morphology of rectangular islands deduced from STM images. The FT spectra of these calculations are shown in Fig. 5(a) and 5(b) (open circles). As a comparison with the calculation for the ideal thin film, we observe that the 2-Å peak narrows and that the height of the 4.4-Å structure lowers. Therefore this simulation nicely reproduces the experimental spectra, because of the reduced lateral and vertical dimensions of the film.

G. Comparison with previous calculations

Recently, two theoretical groups studied the Fe/ZnSe interface. B. Sanyal and S. Mirbt[20] calculated the relaxed positions and the related magnetic properties of the atoms at the interface and in the thin film in the range 0.5–10 ML's. Then, E. Sjösted *et al.*[14] proved that the ideal Fe/ZnSe system do exhibit large in-plane uniaxial magnetic anisotropy (UMA) produced by the directional covalent bonds at the interface, even without atomic relaxation.

The *former* paper described the microscopic mechanism of the observed Se segregation on the surface. Moreover, they calculated that close to the interface Fe atoms are buried inside the substrate. This leads to a slight perturbation of the ideal Fe-crystal structure: all the Fe layers are split into two ~0.1-Å *z*-shifted layers. Even if this last finding is at odds with our experimental results (our Fe layers seem to be more regular), this work succeeds in describing the (2×2) Se superstructure observed in STM images.

The supercell used by Sjöstedt *et al.*[14] in the *latter* paper is very similar to our input file for FEFF: only the floating Se layer differentiates our guess structure from it. In other words, we can say that Fe atoms in the bct planes continue naturally the zinc-blende structure of ZnSe. As a consequence, we can consider that the theoretical findings concerning UMA can be directly compared with magnetic experiences shown in the next section.

III. SECTION II: FERROMAGNETIC RESONANCE EXPERIMENTS (FMR)

The angular dependence of the resonance field permits us, in FMR experiments, to deduce the magnetic in-plane and out-of-plane anistropy constants of thin films.[26] Following the procedure already described, three samples presenting different Fe coverages (4, 6, and 25 ML's) have been prepared. Then, covered by an amorphous ZnSe capping, they were transferred to the *ex situ* FMR setup. The derivative absorption spectra have been obtained with a *X* band VARIAN spectrometer at the frequency 9.25 GHz of the microwave field, the dc field varying in the range 0.2–2.5. Two arrangements of the film sample in a T012 cavity allow an angular variation of the dc field, respectively, in the film plane and in a plane perpendicular to the film.

The FMR experimental results are analyzed using the free-energy density functional:

$$E(\theta,\phi) = -\mathbf{M}\cdot\mathbf{Bext} + \frac{1}{2}\mu_0 M^2\cos^2\theta - \frac{1}{2}K_1^{\perp}\cos^4\theta - \frac{1}{2}K_1^{\parallel}\sin^4\theta(\cos^4\phi + \sin^4\phi) + K_A\sin^2\theta + K_{\mathrm{IP}}\left((1+\sin 2\phi)\frac{\sin^2\theta}{2} - 1\right), \quad (1)$$

where θ and ϕ are the polar and the azimuthal angles of M, the saturation magnetization, with respect to the [100] direction. The first two terms are the Zeeman term and the demagnetization energy. K_1'' and $K_1^{\perp}$ are the in-plane and out-of-plane crystalline anisotropies derived from the cubic magnetocrystalline bulk anisotropy. The last two terms with prefactors K_A, and K_{IP} are the perpendicular and the [110] uniaxial in-plane anisotropy constants.

In the following, we will focus on the in-plane K_{IP} and in the effective out-of-plane magnetic anisotropies ($K_{\mathrm{OP}}=K_A+K_1^{\perp}$).

The angle and frequency dependence of the FMR signal is described using the following law:[27]

$$\left(\frac{\omega}{\gamma}\right)^2 = \frac{1}{M^2\sin^2\theta}\left[\frac{\partial^2 E}{\partial\theta^2}\frac{\partial E}{\partial\varphi^2} - \frac{\partial^2 E}{\partial\theta\,\partial\varphi}\right], \quad (2)$$

where ω is the microwave frequency and γ is the gyromagnetic ratio. From Eq. (2) three equations can be extracted by applying the external magnetic field B_{ext} in the (001) plane along [110] and $[1\bar{1}0]$ (Fe film surface) and out of plane along [001].

The first two equations give the in-plane anisotropy constant K_{IP}, whereas the K_{OP} parameter is obtained from the resonance field value whithin the following approximations:

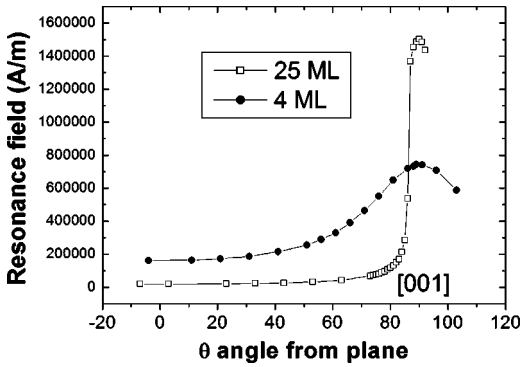

FIG. 6. Angular dependence of the resonance field of 25- and 4-ML- thick layers. Out-of-plane measurements performed at the frequency 9.25 GHz of the microwave field. At $\theta=0$ the magnetic field is along [100] for 25 ML's and $[1\bar{1}0]$ for 4 ML's, easy and hard axis, respectively.

(i) the saturation magnetization values of bulk iron is $M=1.7\times10^6$ A/m (Ref. 8) and (ii) the out-of-plane anisotropy constant is much larger than in plane (shown in the following).

In Fig. 6 we show the out-of-plane measurements and in particular the angular dependence of the resonance field versus the out-of-plane B_{ext} angle. We notice that the resonance field is $\sim1.6\times10^6$ A/m and $\sim8\times10^5$ A/m at 25 and 4 ML's, respectively. These values can be compared with bulk iron in the same configuration, i.e.,$\sim2\times10^6$ A/m. This leads to a rough evaluation of the out-of-plane anisotropy field of 4×10^5A/m at 25 ML's and 1.2×10^6A/m at 4 ML. Moreover, we report that the $K_1^{\parallel}$ cubic constants obtained from fitting are close to those of bulk iron ($\sim4\times10^4$ J/m^3).

In Fig. 7 the in-plane measurements at 6 ML's are reported. We notice that the angular dependence of the resonance field is not symmetric because of the in-plane uniaxial anisotropy favoring the [110] direction. The resonance field difference ΔH between the easy and hard axis is around 8000 A/m. The K_{IP} constant can be estimated as to $\sim10^4$ J/m^3, by $\mu_0\Delta HM/4$. This procedure allows us to extract all anisotropy parameters reported in Table II.

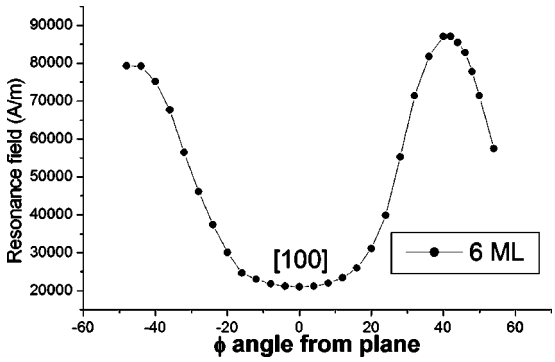

FIG. 7. Angular dependence of the resonance field of 6-ML-thick layers. In-plane measurements were performed at the frequency 9.25 GHz of the microwave field. At $\phi=0$ the magnetic field is along [100].

TABLE II. In-plane and out-of-plane magnetic anisotropy constants, K_{IP} and K_{OP} respectively, evaluated by FMR measurements. We notice that K_{OP} is much larger than K_{IP}.

Anisotropy vs thickness	In plane: K_{IP}(J/m^3)	Out of plane: K_{OP}(J/m^3)
4 ML's	4.6×10^4	1.4×10^6
6 ML's	0.5×10^4	5.6×10^5
25 ML's	2.25×10^3	4.8×10^5

We note that (i) for our thinnest sample (4 ML's) we find that K_{OP} is much larger than K_{IP}: 1.4×10^6 and 4.6×10^4 J/m^3, respectively; (ii) anisotropy terms lower with increasing thickness. These two points will be discussed in the following chapter.

A. Comparison with previous results

Many groups have previously reported the magnetic anisotropy constants of Fe grown by MBE on (001) ZnSe epilayers. In the following a brief state of the art is presented. In a pioneering work J. J. Krebs *et al.*[5] have detected, by vibrating sample magnetometry and FMR, (i) an uniaxial in-plane anisotropy for the thickest layer (137 Å) leading to an inequivalence of the [110] and $[1\bar{1}0]$ directions; (ii) a perpendicular anisotropy whose magnitude decreases with the thickness.

More recently, the magnetic anisotropy constants were measured by Steren *et al.*[28] (FMR on 17- and 90-ML-thick films), by Reiger *et al.*[2] (5.4-, 10-, 17-, and 66-ML-thick films by an alternating gradient magnetometer) and by R. Meckenstock *et al.*[29] (200- and 600-Å-thick films by FMR and superconducting quantum interference device.

After comparison of all these measurements, it turns out that (i) the magnetization lies in the plane and that it is oriented along the [110] direction. (ii) Considering that the bulk g factor is 2.09 and that magnetization is $M=1.7\times10^6$ A/m, we can summarize that for very thin films (under 25 Å) all the measurements gave K_{IP} values of $\sim10^4$ J/m^3, for higher coverages (100–200 Å) K_{IP} starts from $\sim10^3$ J/m^3 (see Ref. 5 and 29) up to $\sim10^4$ J/m^3 (see Ref. 28). These values recover our FMR results obtained on thinner films (Table II). (iii) The out-of-plane uniaxial anisotropy (K_{OP}) is a very important term to the total anisotropy, as reported by Steren.[28]

In the following, we will show that the origin of the perpendicular uniaxial anisotropy resides at the interface between iron and the substrate. Then, we will speculate about the origin of the in-plane anisotropy and we will discuss why this term is one order of magnitude lower than the out-of-plane anisotropy.

B. Origin of the out-of-plane magnetic anisotropy

In order to understand the origin of the important perpendicular uniaxial anisotropy, we focus on two mechanisms that are able to generate an out-of-plane anisotropy: the interfacial and the volume magnetostriction. The *former* is de-

scribed by *Ks* in Eq. (3). It is due to bonding between iron atoms and ZnSe surface. It is important to notice that this parameter does not depend on the film thickness (n_d is the number of atomic layers in the film). The *latter* term, described by *Kv*, is related to the unit-cell distortion due to strain. These two terms add as follows:

$$K = Kv + 2Ks/nd \tag{3}$$

The magnetic anisotropy energy (MAE) in thin magnetic film is in general due to the interface contribution *Ks* since it is much larger compared to the MAE per atom of bulk systems. However, O. Hjortstam *et al.*[30] have shown that if the cubic symmetry of the crystal is broken by a tetragonal distortion, an important contribution to MAE may come from the volume contribution *Kv*. In the case of fct Ni films grown on a Cu(001) substrate, they demonstrated that the observed out-of-plane magnetization is due to the tetragonal distortion.

Since EXAFS experiments indicated that Fe films on ZnSe present a tetragonal distorted structure, it is worthwhile estimating the contribution to MAE due to the volume term *Kv*.

It is known from magnetoelastic theory that the following empirical relation holds:[31]

$$Kv = 3/2\lambda_{001}[C_{11} - C_{12}](\varepsilon_2 - \varepsilon_1). \tag{4}$$

From Sanders[32] we know the elastic constants of the system (C_{11}=229 GPa and C_{12}=134 GPa) and the magnetostriction constant ($\lambda_{001}=24.1\times10^{-6}$), where ε_2 and ε_1 are the strain of the lattice parameter *a* (in plane, along [100]) and *c* (perpendicular to the film surface). From EXAFS measurements, we know that $(\varepsilon_2-\varepsilon_1)$ is almost -1.5%. As a consequence, the volume contribution to MAE of Eq. (4) can be estimated to be 5.4×10^4 J/m^3. Since this value is one order of magnitude smaller than the K_{OP} experimental values (see Table II), we can assume that the *Kv* term due to the tetragonal distortion is irrelevant in respect to the important out-of-plane anisotropy term.

Thus the major contribution comes from the interface term. This result is supported by an another observation: by multiplying by the nominal thickness all the K_{OP} measurements performed previously by other authors on thickest samples up to 600 Å (Refs. 5, 28, and 29), we obtain MAE values between $5-10\times10^{-4}$ J/m^2, sligthly larger than the interface uniaxial magnetic anisotropy measured on Fe/GaAs(001).[13] This corroborates the interfacial origin of the *Ks* term since, as expected by Eq. (3), it does not depend on the film thickness.

C. Origin of MAE and interface atomic structure

We believe that also the in-plane magnetic anisotropy is due to the chemical bonding at the interface between iron atoms and ZnSe. This is supported by a recent theoretical study of MAE performed by E. Sjöstedt *et al.*[14] Indeed, the supercell structure chosen by these authors is very close to our EXAFS experimental results. As a consequence, these theoretical results help us to interprete our findings. E. Sjöstedt *et al.*[14] found that (i) a squarelike interface, broken by the nearest-neighbor semiconducting layer, leads to UMA. (ii) the sp^3-like tetrahedral bonds from the substrate to the Fe atoms at the interface determine the in-plane easy axis: [110] and $[1\bar{1}0]$ for a Se-terminated and a Zn-terminated interface, respectively. (iii) typical MAE values are of 100–300 μeV/interface Fe atom (or $2-6\times10^{-4}$ J/m^2). (iv) the calculated out-of-plane MAE is of the same order of magnitude and in good agreement with the experimental values reported above, i.e., between 5×10^{-4} and 5×10^{-3} J/m^2.

The observed [110] easy axis means that at the interface iron bonds with selenium. As a consequence, at the interface, the semiconductor is either Se terminated or $c(2\times2)$ Zn terminated. Actually, Fe growth is performed on $c(2\times2)$ Zn-terminated surfaces but it is very unlikely that at the interface this superstructure is preserved. Indeed, the interface reactivity leading to the Se-floating layer suggests that (i) the $c(2\times2)$ Zn-ordered configuration must be lost and (ii) 1.5 ML's of zinc is released in the film (not detected by EXAFS). Zinc can form nanoclusters or be substitutional to iron in the film as in Sanyal's model where a layer of Fe and Zn separates the iron film from the substrate.[20] The [110] magnetic easy axis would imply that iron atoms reside mainly in the bonding sites.

D. Why is in-plane magnetic anisotropy lower than out of plane?

In the following, we will put forward two hypothesis to explain why, at odds with theoretical calculations, the measured out-of-plane anisotropy is an order of magnitude larger than the in-plane anisotropy. Both hypotheses, *that are not mutually exclusive*, lower the in-plane anisotropy without modifying the out-of-plane MAE value.

The *former* is related to the *interface layer* Fe and Zn discussed above: a disordered configuration of iron and zinc between bonding and antibonding sites could lead to in-plane MAE values depending on the number of iron atoms occupying the Se-bonding sites and, as a consequence, depending on growth conditions. We notice also that interface disorder could remove the induced and not experimentally observed $\sim$0.1-Å *z* shift of Fe layers discussed in the previous section.

The *latter* hypothesis is related to *the morphology of iron islands* observed by STM. Indeed, STM images show rectangular islands with edges parallel to (110) directions. Elongated edges are mainly aligned along the $[1\bar{1}0]$ directions. Since the demagnetization field H_D differs whether the magnetic field is applied along [110] or $[1\bar{1}0]$, a morphology-induced UMA (shape anisotropy) will lead to an easy axis along $[1\bar{1}0]$ and to a shift of the resonance field equal to $H_D[110]-H_D[110]$. As a consequence, the uniaxial anisotropy constant due to this morphological effect can be calculated by the following magnetostatic model. Let us consider a rectangular plate whose dimensions are *h* (height), *L* (length), and *l* (width) with *L* and $l \gg h$. Similar considerations can be found also in Ref. 33. We can calculate the demagnetization field on an axis parallel to *H*, at the center of the rectangular plate and at *x* from a side perpendicular to *H*. We consider that both sides are composed by two plates

TABLE III. Demagnetization field H_D differs whether the magnetic field is applied along [110] or $[1\bar{1}0]$. This leads to the uniaxial anisotropy constant due to this morphological effect. Let us consider a rectangular plate whose dimensions are h (height), L (length), and l (width) with L and $l \gg h$. We consider that both sides are composed by two wires carrying "magnetic charges" equal to $+Mh$ and $-Mh$, respectively.

Length (L), width (l), and height (h) of islands	$L=20$ Å; $l=15$ Å, $h=3$ Å	$L=50$ Å; $l=35$ Å; $h=3$ Å	$L=200$ Å; $l=140$ Å; $h=3$ Å
Demagnetization field difference: $\Delta H=H_D[110]-H_D[1\bar{1}0]$	75 000 A/m	40 000 A/m	9500 A/m
Morphology-induced anisotropy constant: K_{Shape}	4×10^4 J/m^3	2×10^4 J/m^3	0.5×10^4 J/m^3

carrying "magnetic charges" equal to $+Mh$ and $-Mh$, respectively (See Table III).

We obtain

$$H_D(x) = -\frac{M}{\pi}\left[\sin^{-1}\frac{hl}{\sqrt{(4x^2+l^2)(4x^2+h^2)}} + \sin^{-1}\frac{hl}{\sqrt{[4(L-x)^2+l^2][4(L-x)^2+h^2]}}\right]. \quad (5)$$

At the center of the islands this function is nearly constant. We have calculated the difference $\Delta H=H_D[1\bar{1}0]-H_D[110]$, for three different configurations that are shown in Table III. It can be shown that the morphology-induced anisotropy constant K_{Shape} can be estimated as $\mu_0\Delta HM/4$, within the approximation $2K_{IP}/M \ll 4\pi M$. It is a rough calculation but it allows to compare K_{Shape} with the measured magnetocristalline term K_{IP}: both $\sim10^4$ J/m^3. The K_{shape} term, favoring the $[1\bar{1}0]$, lowers the "real" interface magnetocristalline anisotropy term to the effective K_{IP} term. In other words, the in-plane interface-induced magnetic anisotropy term is much higher than the measured K_{IP} because of the morphology of the iron thin film.

IV. CONCLUSIONS

From STM measurements the picture arising as a whole is consistent with a complex growth characterized by three regimes: at 1 ML Fe forms flat and thin separated metallic islands. Lateral size increases with thickness: at 3 and 5 ML's islands present straight edges along the $\langle 110\rangle$ directions of the substrate. The islands are anisotropic and elongated along $[1\bar{1}0]$ direction. At 7 ML's, the full coalescence is achieved and the roughness is strongly reduced. EXAFS experiments clearly show that iron is strained by epitaxy in a bct structure. For 2- and 4-ML-thick films, a lattice contraction of a equal to -0.025 Å as compared to bulk iron is observed, in good agreement with epitaxy parameters: twice the lattice parameter of Fe ($a_{\mathrm{Fe}}=2.866$ Å) exceeds the lattice parameter of ZnSe ($a_{\mathrm{ZnSe}}=5.669$ Å) by approximately 1.1%. Besides, c is slightly elongated (+0.02 Å).

We have correlated the atomic structure and the morphology of iron thin films with magnetic findings obtained by FMR technique. Our major findings are that the important out-of-plane magnetic anisotropy is due to the interfacial bonding between iron and the substrare rather than to the volume anisotropic term. We have also tried to explain why out-of-plane magnetic anisotropy is larger than in plane. Two hypothesis can be advanced: the *former* is related to a possible disordered configuration of Fe and Zn atoms at the interface between bonding and antibonding sites. The *latter* hypothesis is related to the morphology of $[1\bar{1}0]$ elongated iron islands observed by STM: the demagnetization field H_D differs whether the magnetic field is applied along [110] or $[1\bar{1}0]$, provoking a morphology-induced magnetic in-plane anisotropy term.

We have compared our experimental results with previously reported *ab initio* calculations. In particular we have focused on calculations by Sjöstedt *et al.*[14] of the uniaxial magnetocrystalline anisotropy since the supercell used in this theoretical work is very close to the atomic structure obtained by EXAFS measurements. The magnitude and the direction of calculated magnetic anisotropy corroborates the *scenario* that UMA is due to bonding of interfacial iron atoms with top-most Se-atoms of the ZnSe substrate.

ACKNOWLEDGMENTS

The authors acknowledge B. Sanyal and S. Mirbt for providing calculated atomic coordinates for EXAFS simulations, and the bilateral CAPES-COFECUB program, FAPESP (Grant No. 03/02804-8), CNPq, and French Program Action Concertée Nanosciences-Nanotechologies for financial support.

*Also at Unite Mixte de Physique CNRS-Thales Domaine Corbeville, 91404 Orsay, France and Department of Physics, Uppsala University, Box 530, 75121 Uppsala, Sweden.

†Also at Grupo de Superconductividade e Magnetismo, Centro Multidisciplinar para o Desenvolvimento de Materiais Ceramicos, Departmento Fisica, Universidade Federal de São Carlos, Rodovia Washington Luiz Km 235, Caixa Postal 676, 13565-905 São Carlos, SP, Brazil.

[1] G. Prinz, Science **250**, 1092 (1990).

[2] E. Reiger, E. Reinwald, G. Garreau, M. Ernst, M. Zölfl, F. Bensch, S. Bauer, H. Preis, and G. Beyreuther, J. Appl. Phys. **87**, 5923 (2000).

[3] G. A Prinz, Science **250**, 1092 (1990); R. Fitzgzrald, Phys. Today **53**(4), 21 (2000).

[4] J. M. MacLaren, X.-G. Zhang, W. H. Butler, and Xindong Wang, Phys. Rev. B **59**, 5470 (1999); J. M. MacLaren, W. H. Butler, and X. G. Zhang, J. Appl. Phys. **83**, 6521 (1999).

[5] J. J. Krebs, B. T. Jonker, and G. A. Prinz, J. Appl. Phys. **61**, 3744 (1987).

[6] I. Malajovich, J. J. Berry, N. Samarth, and J. D. Awschalom, Nature (London) **411**, 770 (2001).

[7] X. Jiang, A. Panchula, and S. P. Parkin, Appl. Phys. Lett. **83**, 5244 (2003).

[8] M. Marangolo, F. Gustavsson, M. Eddrief, Ph. Sainctavit, V. H. Etgens, V. Cros, F. Petroff, J. M. George, P. Bencok, and N. B. Brookes, Phys. Rev. Lett. **88**, 217202 (2002).

[9] M. Eddrief, M. Marangolo, S. Corlevi, G.-M. Guichar, V. H. Etgens, R. Mattana, D. H. Mosca, and F. Sirotti, Appl. Phys. Lett. **81**, 4 (2002).

[10] B. T. Jonker and G. A. Prinz, J. Appl. Phys. **69**(5), 2938 (1991).

[11] See, for example, M. Gester, C. Daboo, R. J. Hicken, S. J. Gray, A. Ercole, and J. A. C Bland, J. Appl. Phys. **80**, 347 (1996); M. Zölfl, M. Brockmann, M. Köhler, S. Kreuzer, T. Schweinböck, S. Miethaner, F. Bensch, and G. Bayreuther, J. Magn. Magn. Mater. **175**, 16 (1997).

[12] E. M. Kneedler, B. T. Jonker, P. M. Thibado, R. J. Wagner, B. V. Shanabrook, and L. J. Whitman, Phys. Rev. B **56**, 8163 (1997); R. Moosbühler, F. Bensch, M. Dumm, and G. Bayreuther, J. Appl. Phys. **91**, 8757 (2002).

[13] O. Thomas, Q. Shen, P. Schieffer, N. Tournerie, and B. Lepine, Phys. Rev. Lett. **90**, 017205 (2003).

[14] E. Sjöstedt, L. Nordström, F. Gustavsson, and O. Eriksson, Phys. Rev. Lett. **89**, 267203 (2002).

[15] V. H. Etgens, B. Capelle, L. Carbonell, and M. Eddrief, Appl. Phys. Lett. **75**, 2108 (1999).

[16] L. Carbonell, V. H. Etgens, A. Koëbel, M. Eddrief, and B. Capelle, J. Cryst. Growth **201-202**, 502 (1999).

[17] W. Chen, A. Kahn, P. Soukiassian, P. S. Mangat, J. Gaines, C. Ponzoni, and D. Olego, Phys. Rev. B **49**, 10790 (1994); C. H. Park and D. J. Chadi, Phys. Rev. B **49**, 16467 (1994).

[18] C. Bourgognon, S. Tatarenko, J. Cibert, L. Carbonell, V. H. Etgens, M. Eddrief, B. Gilles, A. Marty, and Y. Samson, Appl. Phys. Lett. **76**, 1455 (2000).

[19] P. M. Thibado, E. Kneedler, B. T. Jonker, B. R. Bennett, B. V. Shanabrook, and L. J. Whitman, Phys. Rev. B **53**, R10481 (1996).

[20] B. Sanyal and S. Mirbt, Phys. Rev. B **65**, 144435 (2002).

[21] D. E. Sayers, E. A. Stern, and F. W. Lytle, Phys. Rev. Lett. **27**, 1204 (1971).

[22] J. J. Rehr, J. Mustre de Leon, S. I. Zabinski, and R. C. Albers, J. Am. Chem. Soc. **113**, 5135 (1991).

[23] D. Chandesris, P. le Fèvre, H. Magnan, A. Chaumin-Midoir, H. Jaffrès, F. Scheurer, and L. Barbier, J. Phys.: Condens. Matter **15**, S657 (2003).

[24] G. Martens, P. Rabe, N. Schwentner, and A. Werner, Phys. Rev. Lett. **39** 1411 (1977).

[25] A. Continenza, S. Massidda, and A. J. Freeman, Phys. Rev. B **42**, 2904 (1990).

[26] M. Farle, Rep. Prog. Phys. **61**, 755 (1998), and references therein.

[27] J. Smit and H. G. Beljers, Philips Res. Rep. **10**, 113 (1955).

[28] L. B. Steren, J. Milano, M. Eddrief, and V. H. Etgens, Physica B **320**, 162 (2002).

[29] R. Meckenstock, D. Spoddif, K. Himmelbauer, H. Krenn, M. Doi, W. Keune, Z. Frait, and J. Pelzl, J. Magn. Magn. Mater. **240**, 410 (2002).

[30] O. Hjortstam, K. Baberschke, J. M. Wills, B. Johansson, and O. Eriksson, Phys. Rev. B **55**, 15026 (1997)

[31] B. Schulz and K. Baberschke, Phys. Rev. B **50**, 13467 (1994); E. W. Lee, Rep. Prog. Phys. **18**, 184 (1955).

[32] D. Sanders, Rep. Prog. Phys. **62**, 809 (1999).

[33] Ch. Bourgognon, Thèse de l'Université J. Fourier, Grenoble 1, France, 2001.